Arbitrary density of states in an organic thin film field-effect transistor model and application to pentacene devices

Daniel Oberhoff, Kurt P. Pernstich, *Student Member, IEEE,* David J. Gundlach, *Member, IEEE,* and Bertram Batlogg

***Abstract*— We present a modular numerical model which allows for an arbitrary densities of states (DOS) for the insulator to semiconductor interface as well as the bulk semiconductor to be independently defined. From this definition we can derive the surface charge density dependence on interface field as well as space charge limited current (SCLC) characteristics. Together with a contact model component we arrive at a physical model which we then apply to a series of staggered inverted (top contact) geometry organic thin film field-effect transistors (OTFTs) with various gate insulator preparations.**

I. INTRODUCTION

OTFTs based on pentacene exhibit a wide range of characteristics. Effective mobilities are usually extracted according to the Schockley model and range up to 5 cm^2/Vs [1], but are typically in the range of 0.1-1 cm^2/Vs. Depending on processing parameters they can operate as depletion or accumulation mode devices. In our devices with a 300 nm thick layer of SiO_2 as gate insulator the turn-on voltage V_{ON}, which we define by the gate voltage at which the device current increases above the measurement noise and leakage currents given sufficient drain voltage (voltages refer to the source), typically varies in the range of -15 to 50 V [2]. The key parameter influencing V_{ON} is the preparation of the gate insulator surface prior to the organic semiconductor deposition. Some correlation can be identified with other parameters such as the field effect mobility (μ_{FET}), subthreshold swing (S), and threshold voltage (V_T) relative to V_{ON} [2].

Several models including or not including percolation, hopping, band transport, trapping/detrapping effects, field activated mobility, traps, or charged grain boundaries in one or two dimensions have been employed previously [3]–[7]. The assumptions on which they are based and their respective histories differ: models assuming disorder and the absence of transport bands usually derive from approaches developed for polymers and models assuming the presence of bands usually derive from amorphous silicon (a-Si) work.

We developed a first principles model based on Fermi statistics in an arbitrary DOS of localized (trap) and delocalized (band) states and monopolar transport (thus excluding bulk recombination effects) via bands of extended states, corresponding to the multiple trapping and release (MTR [8]) picture, and variable range hopping between localized states (VRH [9]). A monopolar model is expected to suffice for the simulation of TFTs with pentacene and numerous other organic semiconductors. In our group, for example, we have not up to now observed both hole and electron transport in a single organic material, independent of the contact metal used. Specifically pentacene has only exhibited hole transport so far. The implementation of our model is strongly based on the approach presented in [4] but we introduced an extended transport model and the possibility to define an arbitrary DOS to account for peculiarities of OTFTs. As in [4] we restrict ourselves to steady state analysis and thereby explicitly neglect charge pumping and other capacitive effects as well as finite trapping/detrapping time constants.

TABLE I

USED SYMBOLS

j	current density
ρ	charge carrier density
F	electric field
ΔF_{int}	dipole induced field at the insulator to semiconductor interface
Ψ_p	hole quasi Fermi level (qfl)
μ	charge carrier drift mobility
ϵ_s	relative dielectric constant of the semiconductor
C_{ox}	capacitance of the gate insulator per unit area
T	thickness of the semiconducting film
W	gate width of the transistor (along the model's symmetry axis)
L	distance between the source and drain contacts
T_{int}	thickness of the interface layer
x_p	position of the pinch-off point along the channel
U_T	thermal voltage k_BT/e where k_B is Boltzmann's constant
ΔL	channel extension length under the contacts
ϕ_b	injection Schottky barrier height
m	Schottky barrier lowering coefficient
R_c	ohmic drain contact resistance
ΔE_P	polaron bandwidth
ΔE_g	polaron band gap
N_P	number of states in the polaron bands per unit volume
V_{deep}	characteristic voltage of the deep state distribution
V_{tail}	characteristic voltage of the tail state distribution
σ_{gauss}	width of the discrete trap level distribution
E_{gauss}	distance of the discrete trap level from the valence band
N_{gauss}	spatial density of states in the discrete trap level
N_0	effective density of states in a Boltzmann approximation
V_{bulk}	voltage at the back of the semiconductor bulk opposite the gate insulator
ΔV_{SCLC}	voltage drop over the bulk transport region
R_0	average carrier localization length in trap states
ν_{ph}	phonon frequency relevant for hopping
f	the Fermi function

II. MODEL DERIVATION

In Figure 1 a schematic of the model is shown where a number of distinct components can be identified: contacts and bulk region, where the bulk is separated spatially into

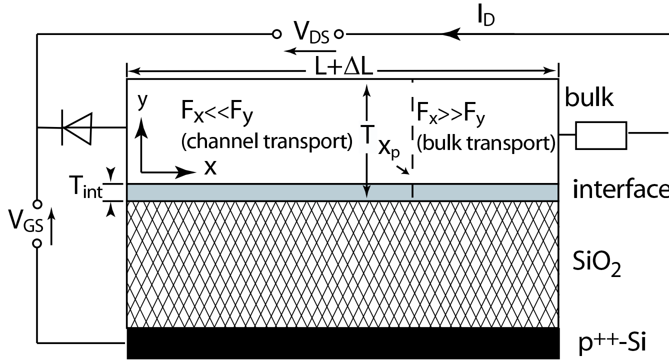

Fig. 1. Model schematic showing the equivalent circuit as well as the different layers of the device and an exemplary separation in channel and bulk conduction regions

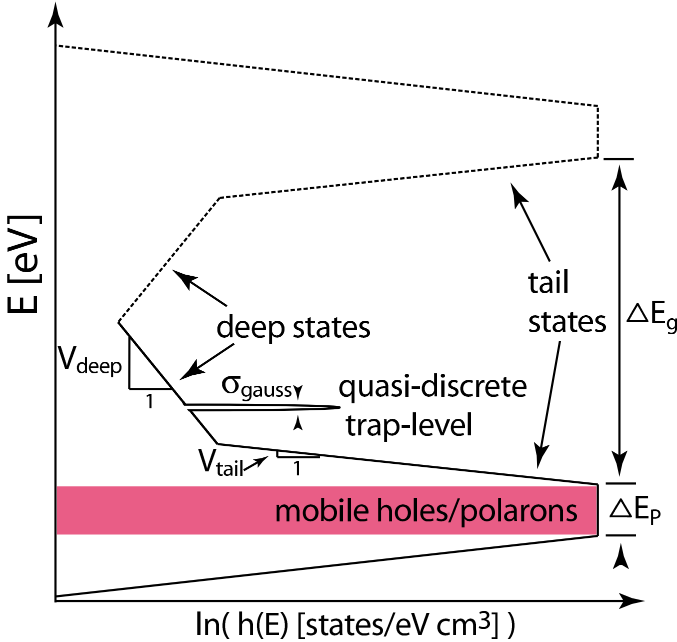

Fig. 2. Prototype of a DOS distribution. Dashed lines indicate electron accepting, full lines indicate electron donating states. Parameter names used in the text and tables are illustrated. Each state can accommodate one charge carrier (electron or hole).

a bulk layer and an interface layer, each with their own DOS, and electrically into channel and bulk transport regions, corresponding to the pre- and post-pinch-off region with the separation line marking the pinch off point x_p. The location of x_p obviously depends on the point of operation of the device. In the following sections we will derive the two conduction models for field effect (FE) and space charge limited current (SCLC) transport both based on Fermi statistics in a mixed MTR/VRH transport model.

A. Bulk model

The basis of the bulk model is the thermodynamical charge distribution statistics given by the Fermi-Dirac statistics: Given a DOS (see Figure 2) and a temperature (which is assumed to be constant throughout the device) it determines the distribution of injected charge among localized and mobile states:

$$\rho_{trapped}(\Psi_p) = \int_{-\infty}^{\infty} h_t(E) f(E - \Psi_p) dE \tag{1}$$

$$\rho_{free}(\Psi_p) = \int_{-\infty}^{\infty} h_f(E) f(E - \Psi_p) dE \tag{2}$$

where h_t and h_f denote the spectral density of localized and extended states respectively. Equations (1-2) determine the free and trapped charge carriers for any Fermi level Ψ_p, and enable us to calculate the contribution of VRH to the net transport. To do the latter we use Mott's expression [9] for the hopping conductivity for low fields ($eFR_0 \ll k_B T$) over a spatial distance R and an energy difference ΔE assisted by phonons of frequency ν_{ph}:

$$\sigma_{VRH}(R, \Delta E) = \frac{2eR^2\nu_{ph}}{U_T} \exp\left(-2\frac{R}{R_0} - \frac{\Theta(\Delta E)\Delta E}{k_B T}\right) \tag{3}$$

where R_0 is the carrier localization length. Averaging over all possible distances and the density of possible initial and final states for hopping yields the VRH-conductivity-contribution as a function of the local hole qfl Ψ_p ($\Theta(x)$ is the unit step function in x):

$$\Delta\sigma_{VRH}(\Psi_p) = \frac{eR_0^2\nu_{ph}}{U_T} \times \tag{4}$$
$$\frac{\iint_{E_V}^{E_C} h_t(E) f(E-\Psi_p) h_t(E') f(\Psi_p - E') e^{-2\frac{\Theta(E-E')(E-E')}{k_B T}} dE dE'}{\int_{E_V}^{E_C} h_t(E) f(\Psi_p - E) dE}$$

where we have assumed a constant localization length R_0 and phonon frequency ν_{ph} resulting in the pre-factor $R_0^2\nu_{ph}$. This introduces a model parameter to which reasonable bounds can be given since it is physical in origin. To arrive at an approximation for pentacene we take the highest intermolecular phonon wavenumber for polyacenes reported in [10] which is $1.2{\cdot}10^3$ cm^{-1} and combine the reported elastic modulus of order 1 GPa [11] and the density of pentacene, which is roughly 1 g/cm^3, to estimate the velocity of sound to be of order 10^5 cm/s. Setting R_0 to the average intermolecular spacing of $\sim 10^{-7}$ cm [10] and assuming linear dispersion then yields a pre-factor of order 10^{-5} cm^2/s. This number, which has the dimension of a diffusivity, is much lower than the diffusivity of the band states in pentacene and thus VRH will only make a significant distribution to current flow where the Fermi level is far from the band and thus in the device off state or beyond the pinch off point. In a device with stronger disorder or lower mobility the situation would be different and hopping would dominate. In theory we can even drop band states and simulate devices with only hopping transport. To account for the VRH conductivity we calculate its effective contribution to the free charge:

$$\rho_{free}^{eff}(\Psi_p) = \rho_{free}(\Psi_P) + \frac{\Delta\sigma_{VRH}(\Psi_p)}{e\mu_0}. \tag{5}$$

The free effective carrier density in equation (5) is not a defined portion of the spatial charge density but an effective

value which preserves the notion of a drift-diffusion-current given by

$$j = W\mu(F\rho^{eff}_{free} - U_T\partial_x\rho^{eff}_{free}) \quad (6)$$

where we have made use of the Einstein-relation. To obtain the sheet carrier density we assume a perfect gate insulator, thus setting $j_y = 0$, and solve the resulting drift-diffusion problem:

$$\partial_y\Psi_p = U_T^{-1}\left(\frac{\partial\Psi_p}{\partial\rho^{eff}_{free}}\rho^{eff}_{free}\right)(\Psi_p)F_y \quad (7)$$

$$\partial_y F_y = \frac{e}{\epsilon_0\epsilon_s}\rho(\Psi_p) \quad (8)$$

for potential differences between the back of the semiconductor bulk (opposite the gate) V_{bulk} and the gate within the experimental range for the respective device, usually 50 to -50 V, and for no transverse electrical field F_y at the back of the device which gives us the second of the necessary two boundary conditions for each solution.

Assuming $F_x \ll F_y$ we can use the solution of equations (7-8) to change variables from x to V_{bulk} to eliminate the spatial derivative in equation to obtain a channel conductivity as a function of V_{bulk} (and implicitly of V_G) which includes diffusive contributions:

$$\sigma^{channel}(V_{bulk}) \equiv W\mu\left(\rho^{eff}_{free,sheet} - U_T\frac{\partial\rho^{eff}_{free,sheet}}{\partial V_{bulk}}\right) \quad (9)$$

where $\rho^{eff}_{free,sheet}$ is the sheet carrier density which is completely determined by equations (1-8) and thereby $\sigma^{channel}(V_{bulk})$ is uniquely determined by the DOS.

On the other hand, when $F_x \gg F_y$ there can be neither drift nor diffusion current in the y-direction so that the Fermi level Ψ_p will be constant in the y-direction and we have:

$$\Delta V_{SCLC} = V_{bulk}(L+\Delta L) - V_{bulk}(x_p) = \int_{x_p}^{L} dx\frac{e\rho}{\epsilon_0\epsilon_s} \quad (10)$$

which we solve by setting $\rho^{eff}_{free} = I_D/WT\mu e\partial_x V_{bulk}$ (neglecting diffusion, see section II-D) which determines ρ through equations (1-2). The resulting partial differential equation (PDE) remains the same (except for a scalar factor c^2 on both sides) under the transformation

$$\begin{aligned} V_{bulk} &\rightarrow c^2 \times V_{bulk} \\ I_D &\rightarrow c \times I_D \\ x &\rightarrow c \times x \end{aligned} \quad (11)$$

which allows us to solve it for any arbitrary x_p and obtain the solution for any other value of x_p from equation (11). x_p, as indicated in Figure 1, is the pinch-off point and determined by $\sigma^{channel}(V_{bulk}(x_p)) = \Delta V_{SCLC}/(L + \Delta L - x_p)$.

Thus we have, for the total voltage drop over the contact-less TFT:

$$\Delta V_{bulk} = \int_0^{x_p} dx I_D/\sigma^{channel}(V_{bulk}(x)) + \Delta V_{SCLC} \quad (12)$$

which implicitly contains I_D and V_G as parameters. We solve the implicit part of this equation by differentiating with respect to x and solving the resulting PDE numerically using the pre-calculated functions derived above. The pinch-off location is determined dynamically in the same step and the SCLC voltage difference added. We thus obtain the solution for the contact-less OTFT in the form $\Delta V_{bulk}(V_G, I_D)$.

B. Contacts

As test sets for our model we have used only data from top contact TFTs in which the depletion width of a possible Schottky barrier is assumed to be always less than the film thickness. Thus to model these devices an undisturbed Schottky barrier is assumed following the standard analytical expression [12]:

$$j_{inj} = 16\pi\epsilon\mu_y U_T^2 N_0\left(e^{\Delta V_{inj}/mU_T} - 1\right) \quad (13)$$

where N_0 is the effective DOS as calculated by a Boltzmann approximation for the injecting contact and μ_y is the mobility in the injecting direction, not necessarily the same as the channel mobility and in the model empirically taken to be reduced by a factor 100 with respect to the transport mobility μ_0 due to the material's anisotropy [13]. m is a constant which encompasses a fist order approximation of bias induced barrier lowering such as that by the image charge seen by a charge carrier approaching the metal. The pre-factor in equation (13) is the effective Richardson constant for low mobility solids as derived in [14]. To account for the area of injection at the contacts we define an injection length which increases the effective channel length.

For the extracting contact we define an ohmic resistance which we treat as a fit parameter. It effectively includes tunnelling as well as interface recombination effects.

C. Charged grain boundaries

It has been suggested that grain boundaries acting as trapping centers will accumulate charge and thus pose a barrier to current flow limiting OTFT current flow [15]. This is naturally motivated by the micro-crystalline patterns observed on thin film micrographs. However it seems unlikely that the observed topography of the pentacene film represents the morphology at the gate insulator where conduction takes place mainly in the first few molecular layers [16], [17]. Also in [1], which lists the highest published field effect mobility to date in pentacene TFTs (measured in saturation), an anti-correlation between grain size and mobility is observed. A similar trend is also indicated in our devices [2]. Models proposed for grain boundaries either require a full 2 dimensional drift diffusion simulation [18] or presume the same Fermi level in the grain boundary as in the grain center [15] which rarely led to meaningful results when inserted into our model.

It is possible to implement a consistent charged grain boundary sub model into our model by defining a DOS for the grain boundary solving for the band bending at the grain boundary in the same step in which band bending at the gate insulator is determined. This would however have multiplied computing times. Considering that grain sizes are usually of order 1 μm $\ll L$ we decided to ignore grain boundary effects in the model, keeping in mind that the overall film morphology will probably enter in the effective values of several of the model's parameters, mainly the band mobility and, in the case of any induced barriers, the Schottky contact injection parameters.

D. Simplifications

1) Throughout we have assumed a constant mobility $\mu = \mu_0$, independent on F, which is a choice we made for the sake of simplicity and to avoid under-determination of the model parameters; it is straightforward and generally unproblematic to add a field dependant mobility to the model and solve the resulting implicit equations.
2) Diffusion is neglected for the SCLC transport mode. This simplification introduces an error of order U_T [19] which can be neglected for organic devices where the voltage needed to raise the measurement signal above the noise level is usually at least of order 1 V.
3) The x and y direction are always treated independently and the Poisson's equation is always only solved for one of these directions. Also no true two-dimensional charge distributions or current flow patterns have been considered. This greatly speeds up simulation times but neglects any intrinsic two-dimensional effects. This introduces errors at the contacts and around the pinch off point at the end of the channel which are expected to be negligible since $T \ll L$. This simplifications also allows us to treat added contacts as in the equivalent circuit shown in Figure 1 just by using Kirchhoff's current law.

III. Application of the Model

For application of the model to TFT data we draw from a data set from our group which has been presented and analyzed in [2]. To demonstrate and test the model we chose devices, which differ in the way the gate insulator is treated before deposition of the pentacene film: a phenyl-trichlorosilane (PTCS) treated device which turns on nearly exactly at zero gate bias and a perfluorooctyl-trichlorosilane (PFTCS) treated device turning on around $V_G = 50V$. The simulations took about five minutes each on a 2 GHz Pentium 4 using MATLAB R14SP1 and are thereby much faster than any full 2d simulation especially considering that all the code is running on an interpreter (MATLAB) and is never compiled into machine code.

To fit the simulation to the data we chose parameters which would produce good fits for both the measured saturation transfer and the output characteristics.

TABLE II
Geometric constants and assumed material parameters for the modelled pentacene devices

parameter	value	source
T [1]	20 nm	empiric [1]
W	600μm	measured
L	30 μm	measured
T_{int} [2]	1.5 nm	empiric[2]
ΔL	40 μm	[20]
C_{ox}	$1.2{\cdot}10^{-8}$ F/cm^{-2}	measured
ΔE_P	300 meV	[21]
ΔE_g	2.25 eV	[10]
N_P	$5.4{\cdot}10^{21}$ cm^{-3}	[10], [22]
ϕ_b	0.3 eV	empiric
ϵ_s	3	[23]

Some parameters where kept constant during the course of fitting, including geometric constants and assumed material parameters (see Table II, with references to published values where appropriate). The injection barrier was treated as a fit parameter but held constant for both device simulations. 300 K was assumed for the ambient temperature. The DOS was always composed of rectangular bands (for a discussion of the band shape see section I) with exponential tail states of variable steepness V_{tail} to model the above threshold characteristics but always symmetric with respect to the band gap center and always the same in the bulk and the interface layer (see Figures 1 and 2). To model subthreshold characteristics and off-current we introduced deep states with exponential DOS of characteristic steepness V_{deep} and spatial density N_{deep}, again symmetric with respect to the band gap center but with different steepness and spatial density for the bulk and the interface layer. The interface layer DOS had a stronger effect on the subthreshold behavior while the in the bulk layer DOS is used to control the off currents and also, to some extent, the subthreshold behavior. Additionally to reproduce step like artifacts in the subthreshold characteristics of the PTCS treated device we introduced a trap level with Gaussian DOS of width σ_{gauss}, energy position E_{gauss} (with respect to the valence band), and spatial density N_{gauss}. All these components are illustrated in Figure 2.

TABLE III
Parameters used in the simulations of the pentacene TFTs

parameter	unit	PTCS device	PFTCS device
ΔF_{int}	$[MV/cm]$	0.005	-2.45
V_{tail}	$[meV]$	34	37
$N_{deep}^{interface}$	$[cm^{-3}]$	$2{\cdot}10^{17}$	$1{\cdot}10^{19}$
$V_{deep}^{interface}$	$[meV]$	240	180
N_{deep}^{bulk}	$[cm^{-3}]$	—	$9{\cdot}10^{16}$
V_{deep}^{bulk}	$[meV]$	—	400
E_{gauss}	$[eV]$	0.42	—
N_{gauss}	$[cm^{-3}]$	$2{\cdot}10^{17}$	—
σ_{gauss}	$[meV]$	2	—
μ_0	$[cm^2/Vs]$	12.8	5.5
R_c	$[k\Omega cm]$	1.0	13.0
m	$[1]$	7	7
$R_0^2\nu_{ph}$	$[cm^2/s]$	10^{-4}	$5{\cdot}10^{-5}$

Figure 3 shows the measured transfer characteristics for both devices with the corresponding simulation results superimposed. Parameters where optimized to fit both the subthreshold region of the transfer characteristics and the measured output characteristics (see figures 4 and 5). The quality of the over-all fits is very good, including several subtleties in the transfer and output characteristics. The tail width parameter V_{tail} and the is very similar in both devices as might be expected on physical grounds while the band mobility is different by a factor ~ 2 which could be due to a different mixture of phases with different intermolecular spacing in

[1] the nominal value is 40 nm but we only expect about halve of this to be effective for transport because of a significant surface roughness [2]. Note that the parameter T is only significant for SCLC transport.

[2] The value 1.5 nm for T_{int} corresponds roughly to a molecular monolayer of pentacene [10].

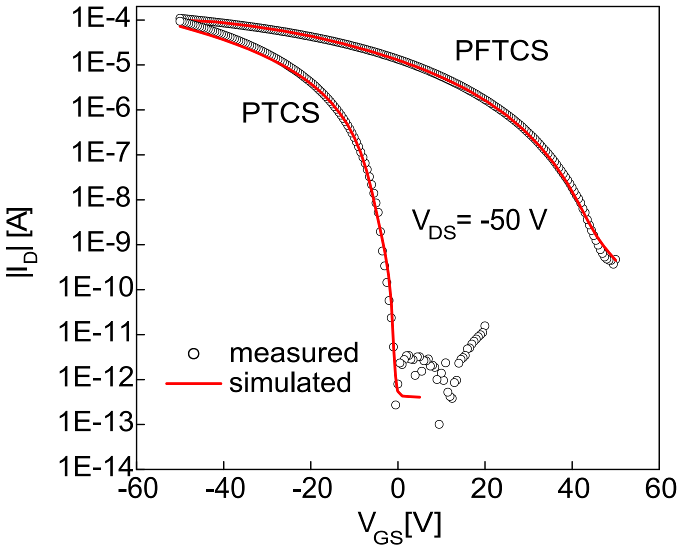

Fig. 3. Measured and simulated transfer characteristics of the PTCS and the PFTCS device; V_{DS} was $-50V$. The parameters are optimized to fit the subthreshold region of these characteristics and output characteristics on a linear scale (see figures 5 and 4), that is from turn on to about 5-10 V below turn on. The above threshold region is subject to hysteresis (discussion in the text). The characteristics converge around 0.1 mA which is $\sim$ 10% of the intrinsic limit for this geometry at an assumed mobility of $\sim$ 10 cm^2/Vs.

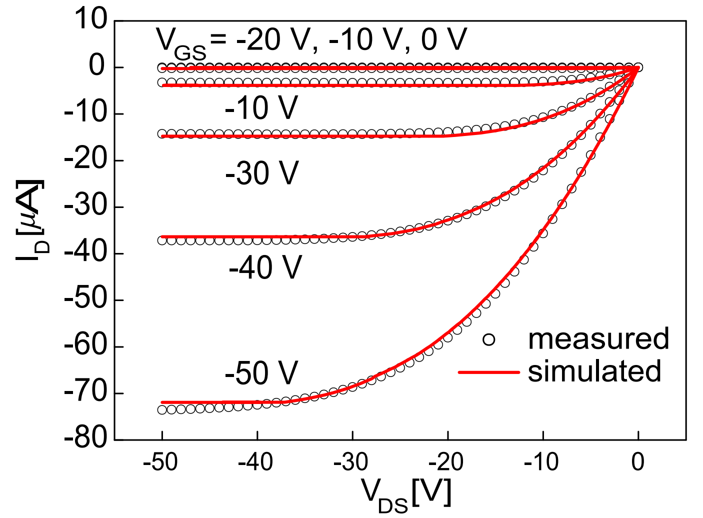

Fig. 4. Output characteristics of the PTCS treated device; V_{DS} was varied in $-10V$ steps from $0V$ to $-50V$. Simulation results are shown. The device saturates fully over the whole applied bias range. A very good overall fit is achieved. A turn-on nonlinearity is present but barely noticeable because the characteristics quickly bend over into saturation, indicating that current is mostly limited by the bulk and not the contacts. Compare to Figure 5.

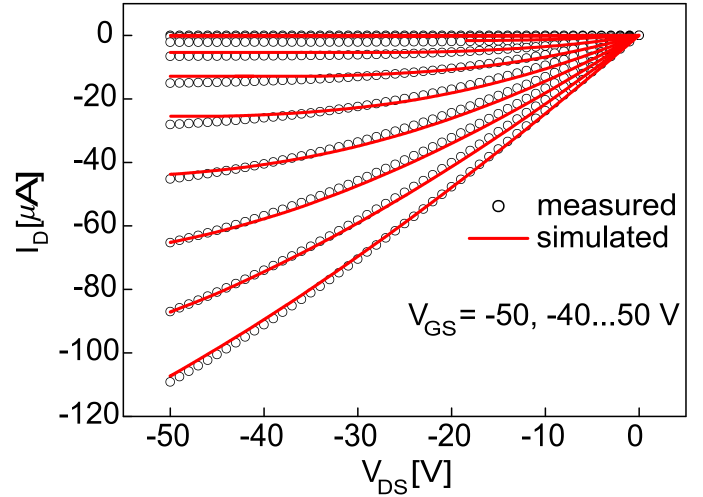

Fig. 5. Output characteristics of the PFTCS treated device; V_{DS} was varied in $-10V$ steps from $50V$ to $-50V$. Simulation results are shown. Strong ohmic injection limiting, typical for defective Schottky barriers [12], and the increase of the effective gate bias due to the interface field hinder saturation of this device. Due to this the turn-on non-linearity, which is in fact weaker than for the PTCS device, is more visible.

the film [2] and the fact that this number is an effective number subsuming a number of not modelled effects such as grain boundaries. The mobility entering the model is in both cases about ten times higher than the mobility extracted using a simple Schockley model (0.71 and 0.15 cm^2/Vs for the PTCS and PFTCS device respectively). This factor is reflected in the model by the ratio of injected to effectively mobile charge in the above threshold regime (see Figures 6 and 7). The simulation parameters used for the fit are listed in Table III. The fits exhibit an absolute accuracy $\sim$ 1 μA and a relative accuracy $\sim$ 10% for the output characteristics and a relative accuracy $\sim$ 5% for the saturation transfer characteristics. The error in the output characteristics probably arises mainly from the total neglect of film inhomogeneities such as grain boundaries in the transport direction. The error in the transfer characteristics occurring in the large negative gate bias region, where it is largest, originates mainly from hysteretic effects which cause lower saturation currents in the output measurement, which where measured last, than in the saturation transfer measurement, which where measured first.

As seen in Figure 3 both saturation transfer characteristics converge at around 100 μA but turn on at a very different gate bias. This was modelled by defining built-in fields ΔF_{int} for both devices. The physical origin of ΔF_{int} is assumed to be the dipole field of the corresponding gate insulator surface treatment agent (for a more thorough discussion see [2]). While this dipole field is negligible for the PTCS treated device, it is $\sim$ 2.5 MV/cm in the device treated with PFTCS, forming a strong dipole due to the dissimilar endgroups of the molecules. We also tried to model the shift using acceptor states (doping) as was done in [3]. We could not reproduce their results in our model: generally had problems maintaining the subthreshold slope and the off-current level with the acceptor states. But this might also be due to the fact that we did not implement electron transport while one would expect hopping among the acceptor sites.

The PFTCS characteristics seem to be 'stretched' compared to the PTCS characteristics. Also the currents in the off state differ by several orders of magnitude. This was modelled by a deep trap density which is almost three orders of magnitude higher in the PFTCS device than in the PTCS device. This makes the PFTCS treated device almost ohmic in its off-state because the relatively wide trap state distribution around mid gap makes a large contribution to the effective free carrier density via the VRH mechanism. The hopping diffusivity was chosen slightly different for the two devices to account for

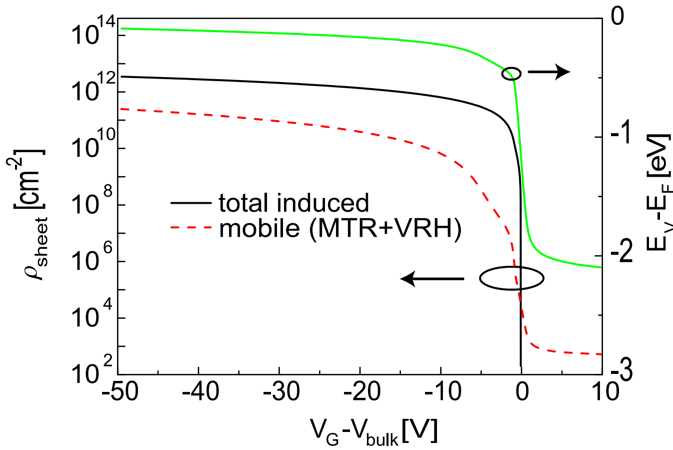

Fig. 6. Bias dependance of the total induced and the effectively mobile charge carrier density for the PTCS device (MTR and VRH contributions). Also shown is the corresponding Fermi level at the insulator. One can extract a maximum charge injection efficiency of around 10%. The gaussian trap level introduces a noticeable kink in the dependency of the mobile sheet carrier density on the gate to bulk voltage. Compare to Figure 7.

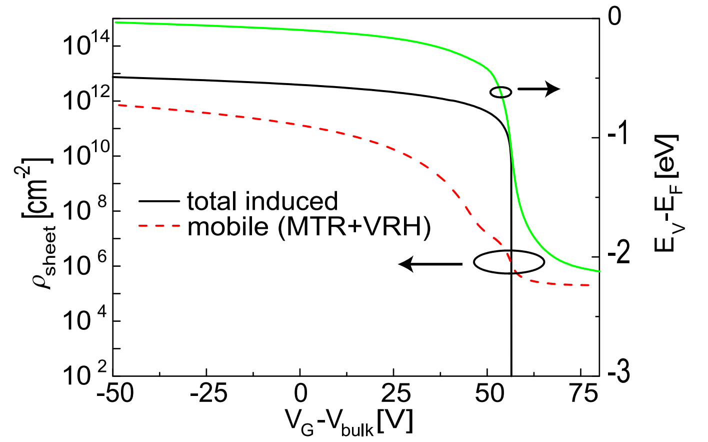

Fig. 7. Bias dependance of the total induced and the effectively mobile charge carrier density for the PFTCS device (MTR and VRH contributions). Also shown is the corresponding Fermi level at the insulator. One can extract a maximum charge injection efficiency of around 10%. The high density of deep states weakens the sensitivity of both the mobile sheet carrier density and the Fermi level at the interface on the gate-to-bulk voltage. Compare to Figure 6.

phases with different intermolecular spacings in the films. The physical origin of the deep states could be structural or linked to a change in the effective charge carrier (see section II). The PTCS characteristic shows a soft step in the subthreshold region. This effects was modelled by introducing a quasi discrete trap level close to 0.4 eV from the valence band which is in agreement with observations in [24]. It is possible that the above mentioned hysteresis originates in the meta-stability of this trap level [24]. Further insight is gained through Figures 6 and 7 where the bias dependance of the total induced charge carrier density and effective mobile charge carrier sheet density are shown, as well as the Fermi level at the gate insulator.

Figures 4 and 5 show the output characteristics of the devices. This data was used to determine contact parameters as well as, to some extent, the tail state steepness and the mobility. The two devices differ mainly in ”extrinsic” parameters such as the interface and the deep states as well as the contact parameters. The PFTCS device does not fully saturate at high gate bias. We explain this by a large contact resistance as well as by the strong built-in field induced by the surface treatment. This built-in field shifts the characteristics about 50 V towards positive gate bias, thus a nominal gate-to-source bias of -50 V has the same effect as a -100 V bias in a device with no built-in field which is much higher than the applied drain to source voltage and thus the device fails to saturate. A non-linear turn-on is seen for both devices (though it is more visible for the PFTCS device due to the lack of saturation) and is modelled with the same injection contact Schottky barrier non-ideality parameter m as the PTCS device which indicates that the contact barrier lowering mechanism is the same for both devices.

IV. Conclusions

We have presented a simple model based on the Maxwell equations and Fermi statistics of the charge carriers and a mixed multiple trapping and release/variable range hopping transport model including drift and diffusion currents and allowing for an arbitrary DOS and a number of other physical parameters. We have applied it successfully to differently prepared thin film devices and estimated the physical parameter ranges of these devices yielding very reasonable values for these parameters.

We have explained the turn-on dynamics in terms of SCLC conduction and VRH contributions and pointed out that mobility values extracted using a Schockley model seem typically smaller than the intrinsic mobilities by a factor of order of the ratio between induced and effectively free charge which is typically of order 10 for devices like the ones presented based on pentacene.

For a fuller understanding of interface effects (as well as long term hysteretic effects which are most probably strongly linked with the latter) a detailed theoretical study has yet to be carried out concerning chemical reactions at the interface in the presence of a strong electric field, an electrochemically active silane coupling agent introduced by the surface treatment, and chemical impurities in the bulk material as well as the ambient atmosphere. In addition the real geometric properties of the interface between the gate insulator (plus additional surface layer) and the organic semiconductor as well as the details of the hopping mechanism need further consideration. The latter effects are currently subsumed in the transport mobility μ_0 and the hopping pre-factor $R_0^2\nu_{ph}$. Furthermore it is probable that the DOS extracted using our model differs from the single electron (or single hole) DOS because charge is transported in polarons which are known to be sensible at least to temperature and spatial anisotropy [10], [21], [25]. It is possible that the change in DOS at the interface is induced by a change in the configuration of the polaron (see for example [26]. It would be particularly interesting to measure the DOS independently using spectroscopic methods and compare it to the model DOS.

In conclusion we have achieved remarkable fit qualities for

both transfer and output characteristics with a rather simple physical theory of the device operation. We allow for an arbitrary density of states containing extended state bands, shallow tail states, and deep trap states (wide as well as discrete) in a mixed multiple trapping and release/variable range hopping transport model employing numerical solutions of differential equations in only one spatial dimension.

APPENDIX I
DISCUSSION OF THE BAND SHAPE

In no simulated device at any realistic point of operation did the hole qfl come closer to the mobility band edge than a few thermal voltages ($U_T = k_B T$). Thus the amount of band carriers as a function of the hole qfl can always be sufficiently approximated by the usual Boltzmann law:

$$\rho_{free} = \rho^0_{band} \cdot e^{\frac{\Psi_p - \Psi^0_p}{U_T}} \tag{14}$$

where all the information about the band reduces to the numerical pre-factor ρ^0_{free} which is known as the effective DOS in classical semiconductor theory. The amount of uncertainty is increased by the fact that the only way we can measure the free carrier density is via the induced conductivity which is also proportional to the free carrier mobility which is, in principle, an unknown quantity. This means there is little point in assigning much detail to the band shape used in the simulation and we thus decided to stick to the rectangular shape with a bandwidth of 0.3 eV for pentacene, the latter chosen based on calculations in [27]. Changing the bandwidth or putting more detailed structure to it will move its weight relative to the mobility edge and change the effective DOS which would require us to correct the band mobility accordingly to obtain the same simulation results.

Another aspect we want to touch here for the sake of completeness is the quantization of the DOS as charge is confined in a more and more two dimensional arrangement as is the case at the gate insulator of an operating TFT. The following equation yields the quantization steps of the DOS at the gate insulator as a function of the interface field and the transverse effective charge carrier mass (in the triangular potential approximation):

$$E_n = \left(\frac{\hbar^2}{2m_\perp}\right)^{1/3} \left(\frac{3\pi e F}{2}\left(n + \frac{3}{4}\right)\right)^{2/3}. \tag{15}$$

For typical fields of order MeV/cm this yields energy steps of order 10-100 meV. This quantization effect could further reduce the effective DOS and thus lead to underestimating the mobility.

APPENDIX II
DISCUSSION OF THE EFFECTIVE CHARGE CARRIER AND ITS MODE OF TRANSPORT

In organic molecular crystals the bonding forces are weaker than in conventional inorganic semiconductors. In pentacene, where bonding is of van der Waals (VdW) type, it is typically only 10-100 meV [10] per bond which is much weaker than covalent bonds in, say, silicon based semiconductors which results in a much smaller transfer integral and therefore in a strongly reduced transport bandwidth. In the past transport has usually been assumed to be incoherent and field activated mobilities have periodically been proposed. We have, however, not found it necessary to use a field-dependant mobility in the simulations of the presented devices. This is probably due to the fact that we have restricted modelling to relatively long channel devices where the transporting field is low making it possible to treat it as a small perturbation only. On the other hand in the lateral direction perpendicular to the gate insulator fields are very high and it is possible that the drift diffusion balance used to obtain the charge distribution should correctly be modified. In the past a Pool-Frenkel kind of modification has been brought forward [28] which might have to be applied for discrete trap levels such as the one used to fit the PTCS device. The effect of this would be to increase the number of these states to have the same effect in the simulation. We do not see how this effect would be applicable to wide distributions since the picture of a singular attracting potential on which the Pool-Frenkel idea is based does not hold in this case.

Generally, a transport band of coherent states is expected to exist at least for high mobility devices. This is supported by theory which suggests that at high temperatures, as the mean free path of the bare charge carrier drops below the intermolecular distance, polarons bands of considerable width form [10], [21], [25]. This is supported by measurements of temperature dependance of mobility for high mobility devices [29] which match predictions and the displayed series can be interpreted as a crossover from incoherent to coherent transport (going from low to high mobility devices). This justifies our choice of a mixed VRH/MTR transport model.

APPENDIX III
RELEVANT NUMERICAL IMPLEMENTATION DETAILS

To perform the convolution of the DOS with the Fermi function we point-sample the integrand with a high density and integrate using the Simpson rule. To solve the boundary value problem arising in the FE transport mode (equations 7 and 8) we use MATLAB's bvp4c routine which implements a collocation based algorithm. To solve the transport PDE's (equations 10 and 12) we use MATLAB's ode15s routine which proved to be the the most robust of its initial value problem (IVP) solvers. To store and retrieve pre-calculated functions we use an essentially non oscillatory (ENO) interpolation method, which is similar to a Newton interpolation but the points added at every order to compute the higher derivatives are chosen in a manner as to obtain the smoothest possible interpolant, on a look-up table of sampled values. The ENO scheme avoids artificial oscillations arising at discontinuities caused for example by a rough sketching of the DOS and guarantees smoothness right up to such a discontinuity (as long as enough sample points are available) and will usually only oscillate when the function itself is oscillatory.

ACKNOWLEDGEMENTS

The authors would like to thank Benjamin Rössner, Cornelius Krellner, Libero Zuppiroli, Gilles Horowitz, and

Thomas Jackson for fruitful discussions.
This study is partly supported by ETH grant 20020-02, by the Swiss National Science Foundation, and by the Swiss BBW as part of the EU-Research program EUROFET (HPRN-CT-2002-00327).

REFERENCES

[1] T. W. Kelley, D. V. Muyres, P. F. Baude, T. P. Smith, and T. D. Jones, "High performance organic thin film transistors," *Mat. Res. Soc. Symp. Proc.*, vol. 771, p. L6.5, 2003.
[2] K. P. Pernstich, A. N. Rashid, S. Haas, G. Schitter, D. Oberhoff, C. Goldmann, D. J. Gundlach, and B. Batlogg, "Threshold voltage shift in organic field effect transistors by dipole monolayers on the gate insulator," *J. Appl. Phys.*, vol. 96, no. 11, p. 6431, December 2004.
[3] A. R. Völkel, R. A. Street, and D. Knipp, "Carrier transport and density of state distributions in pentacene transistors," *Phys. Rev. B*, vol. 66, p. 195336, November 2002.
[4] P. Servati, D. Striakhilev, and A. Nathan, "Above-threshold parameter extraction and modeling for amorphous silicon thin-film transistors," *IEEE Trans. Electron. Dev.*, vol. 50, no. 11, p. 2227, November 2003.
[5] M. Koehler and I. Biaggio, "Space-charge and trap-filling effects in organic thin film field-effect transistors," *Phys. Rev. B*, vol. 70, p. 045314, July 2004.
[6] T. Lindner and G. Paasch, "Influence of distributed trap states on the characteristics of top and bottom contact organic field-effect transistors," *J. Mater. Res.*, no. 7, p. 2014, February 2004.
[7] M. A. Alam, A. Dobalapur, and M. R. Pinto, "A two-dimensional simulation of organic transistors," *IEEE Trans. Electron. Dev.*, vol. 44, no. 8, p. 1332, August 1997.
[8] G. Horowitz and M. E. Hajlaoui, "Grain size dependent mobility in polycrystalline organic field-effect transistors," *Synth. Met.*, vol. 122, no. 1, p. 185, May 2001.
[9] N. F. Mott and E. A. Davis, *Electronic processes in non-crystalline materials*, 2nd ed., ser. Monographs on Physics, W. Marshal and D. H.Wilkinson, Eds. Oxford: Clarendon Press, 1979.
[10] E. A. Silinsh and V. Čápec, *Organic Molecular Crystals*. New York: AIP Press, 1994.
[11] L. F. DRummy, P. K. MIska, and D. C. Martin, "Plasticity in pentacene thin films," *J. Mat. Sci.*, vol. 39, p. 4465, 2004.
[12] E. H. Rhoderick and R. H. Williams, *Metal-Semiconductor contacts*, 2nd ed. Oxford: Clarendon Press, 1988.
[13] N. Karl, "Charge transport in organic solids," *Synth. Met.*, vol. 113-114, p. 649, 2003.
[14] J. C. Scott and G. G. Malliaras, "Charge injection and recombination at the metal-organic interface," *Chem. Phys. Lett.*, vol. 299, no. 2, p. 115, January 1999.
[15] G. Horowitz, "Tunneling current in polycrystalline organic thin-film transistors," *Adv. Funct. Mat.*, vol. 13, no. 1, p. 53, January 2003.
[16] D. J. Gundlach, C.-C. S. Kuo, C. D. Sheraw, J. A. Nichols, and T. N. Jackson, "Improved organic thin film transistor performance using chemically modified gate dielectrics," *Proc. SPIE*, vol. 4466, p. 54, December 2001.
[17] R. Ruiz, B. Nickel, N. Koch, L. C. Feldman, R. F. Haqlund, A. Kahn, and G. Scoles, "Pentacene ultrathin film formation on reduced and oxidized si surfaces," *Phys. Rev. B*, vol. 67, p. 125406, March 2003.
[18] F. M. Hossain, J. Nishii, S. Takagi, A. Ohtomo, T. Fukumura, F. Fujioka, H. Ohno, H. Koinuma, and M. Kawasaki, "Modeling and simulation of polycrystalline zno thin-film transistors," *J. Appl. Phys*, vol. 94, no. 12, p. 7768, December 2003.
[19] W. Helfrich, *Physics and Chemistry of the Organic Solids*, 2nd ed. Interscience Publishers, 1988, vol. 3, ch. Space-charge-limited and volume-controlled currents in organic solids.
[20] D. J. Gundlach, "Small-molecule organic thin film transistors," Ph.D. dissertation, Pennsylvania State University, University Park, PA, 2001, 2001.
[21] K. Hannewald, V. M. Stojanović, J. M. Schellekens, P. A. Bobbert, G. Kresse, and J. Hafner, "Theory of polaron bandwidth narrowing in organic molecular crystals," *Phys. Rev. B*, vol. 69, p. 075211, February 2004.
[22] D. Knipp, R. A. Street, A. Völkel, and J. Ho, "Pentacene thin film transistors on inorganic dielectrics: Morphology, structural properties, and electronic transport," *J. Appl. Phys*, vol. 93, no. 1, p. 347, January 2003.
[23] M. Schubert, C. Bundesmann, G. Jacopic, H. Maresch, and H. Arwin, "Infrared dielectric function and vibrational modes of pentacene thin films," *Appl. Phys. Lett.*, vol. 84, no. 2, p. 200, January 2004.
[24] D. V. Lang, X. Chi, T. Siegrist, A. M. Sergent, and A. P. Ramirez, "Amorphouslike density of gap states in single-crystal pentacene," *Phys. Rev. Lett.*, vol. 93, no. 8, p. 086802, August 2004.
[25] D. Emin, "Correlated small-polaron hopping motion," *Phys. Rev. Lett*, vol. 25, p. 1751, December 1970.
[26] M. N. Bussac, J. D. Picon, and L. Zuppiroli, "The impact of molecular polarization on the electronic properties of molecular semiconductors," *Europhys. Lett.*, vol. 66, no. 3, p. 392, 2004.
[27] K. Hannewald and P. A. Bobbert, "Anisotropy effects in phonon-assisted charge-carrier transport in organic molecular crystals," *Phys. Rev. B*, vol. 69, p. 075212, February 2004.
[28] Rashmi, V. R. Balakrishnan, A. K. Kapoor, V. Kumar, S. C. Jain, R. Mertens, and S. Annapoorni, "Effect of field dependent trap occupancy on organic thin film transistor characteristics," *J. Appl. Phys.*, vol. 94, no. 8, p. 5302, October 2003.
[29] S. F. Nelson, Y.-Y. Lin, D. J. Gundlach, and T. N. Jackson, "Temperature-independent transport in high-mobility pentacene transistors," *Appl. Phys. Lett.*, vol. 72, no. 15, p. 1854, April 1998.

Kurt P. Pernstich Kurt P. Pernstich received the M.Sc. degree in Electrical Engineering in 2002 from Graz University of Technology. In the same year he started his Ph.D. studies in the Laboratory for Solid State Physics at ETH Zrich. He works mainly with organic field effect transistors to investigate physical properties of organic materials.

Daniel Oberhoff Daniel Oberhoff received the Diploma in Physics in 2004 from the ETH Zurich where he spent over a year in the "Physics of New Materials" group of the solid state physics department working on the characterization and simulation of organic electronic devices. He is interested in applying interdisciplinary approaches to fundamental questions in theoretical as well as experimental physics usually with the help of the computer and is planning to begin Ph.D. studies in physics in fall 2005.